3.40

A FACILITY FOR LOW ENERGY CHARGED PARTICLE INDUCED REACTION STUDIES

T. Vilaithong, S. Singkarat, L.D. Yu, S. Intarasiri and U. Tippawan
Fast Neutron Research Facility, Department of Physics, Faculty of Science,
Chiang Mai University, Chiang Mai 50200, Thailand
e-mail: fnrf@loxinfo.co.th

Abstract

In Chiang Mai, a highly stable low energy ion accelerator (0 − 350 kV) facility is being established. A subnano-second pulsing system will be incorporated into the beam transport line. The detecting system will consist of a time-of-flight charged particle spectrometer and a high resolution gamma-ray system. The new facility will be used in the studies of low energy heavy ion backscattering and charged particle induced cross section measurement in the interests of material characterization and nucleosynthesis.

1 INTRODUCTION

In order to develop ion beam analysis techniques in the laboratory by giving further play to the potential of present research facilities instead of generous investing and installing new facilities, we introduce the time-of-flight (TOF) analyzing technique but using backscattering of low-energy ion beams [1]. The technique is considered to be a new ion beam analysis technique, different from using conventional high or medium energy ion beams, specially benefiting compositional and depth-profiling analysis of thin films, ion-implanted layers and deposited thin coatings. The basics of the technique is Rutherford Backscattering Spectrometry (RBS) [2], however, the traditional detection is revolutionized to be the time-of-flight method, which then provides an unprecedented resolution of energy or mass. The techniques to be applied in the composite facility include the pulsed beam TOF-RBS, low-medium-energy RBS, (p,γ) & $(p,\alpha\gamma)$ reaction, and E & ΔE spectrometry.

2 FEATURES OF LOW-ENERGY-ION-BEAM RBS ANALYSIS

2.1 Ion Beam Conditions Currently Available at FNRF

Figure 1 shows the present 150-kV accelerator-based neutron generator [3], which is to be modified for the purpose of low energy charged particle induced reaction studies.
The ion beam conditions available at the facility are listed below.

Ion:	H^+, D^+, He^+, He^{2+}
Accelerating voltage:	200 kV (maximum)
Mass-analysis bending angle:	90°
Beam pulse:	1.5 ns
Target chamber vacuum:	$10^{-6} - 10^{-5}$ Torr

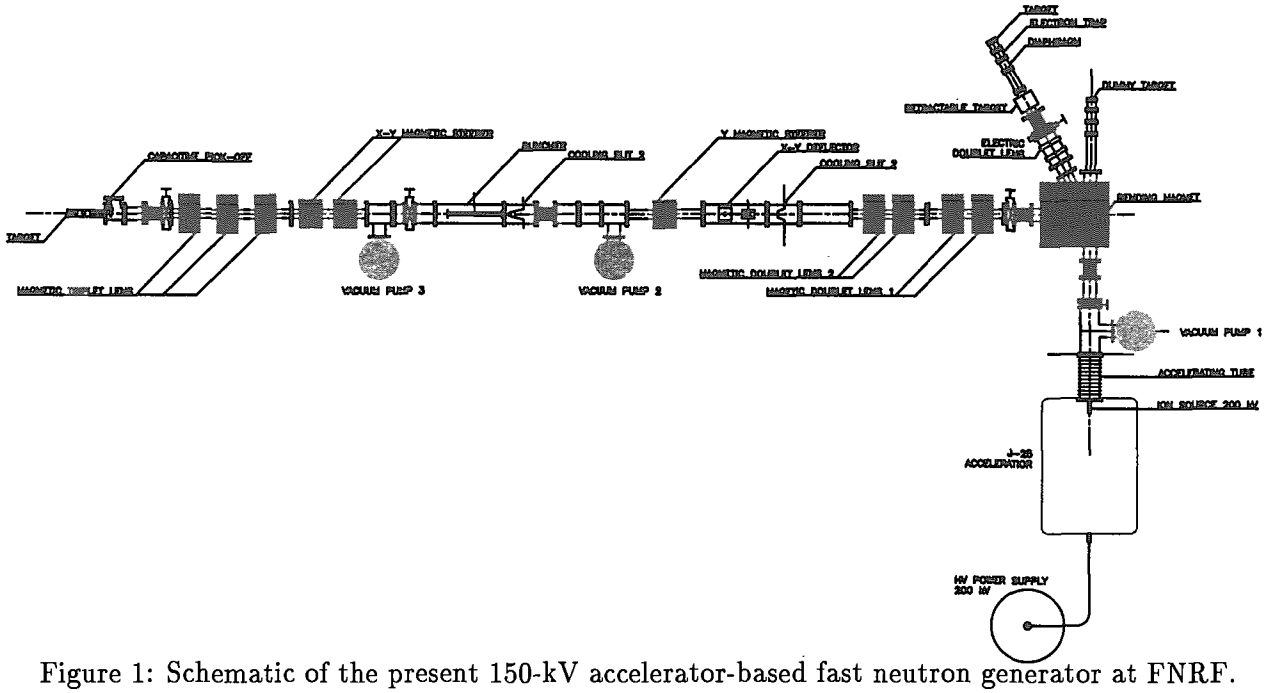

Figure 1: Schematic of the present 150-kV accelerator-based fast neutron generator at FNRF.

2.2 Features of Low-Energy RBS

Table 1 lists the calculated/estimated results for H^+, D^+, He^+ and He^{2+} ions accelerated by 150 kV (the actual energy of He^{2+}-ion is then 300 keV) analyzing (a) Si and (b) Fe with 0°-incident-angle and 150°-scattering-angle [4,5,6,2,7]. The resolvable mass difference from the target-mass is based on a 5-keV energy resolution of a silicon surface barrier detector. For comparisons, the results from 2-MeV H^+ and He^+ ions and 600-keV He^{2+} ion are also listed. In the case of 2 MeV, the energy resolution is used as 15 keV; in the case of 600 keV, the energy resolution is taken as 8 keV. σ: Scattering cross section; R: Projected range; K: Kinematic factor; d_a: Maximum analyzing depth; r_m: Mass resolution; ΔM_2: Resolvable mass difference from the target-atom mass M_2. D^+ is emphasized as it is primarily considered as the standard ion beam.

Table 1. Features of Low-Energy RBS.

(a) Target: Si

Ion	H^+	H^+(2MeV)	D^+	He^+	He^+(2MeV)	He^{2+}	He^{2+}(0.6MeV)
$\sigma(10^{-10}\mathrm{nm}^2)$	12.9	0.07	**12.8**	50	0.28	12.4	3.1
R(nm)	1,238	46,300	**990**	840	6,800	1,300	2,120
K	0.8752	0.8752	**0.7658**	0.5845	0.5845	0.5845	0.5845
d_a(nm)	400	20,000	**370**	350	2,500	400	800
$r_m(\frac{\Delta E_1}{\Delta M_2})$	0.71	9.5	**1.43**	2.85	38	5.7	11.4
ΔM_2	7	1.6	**3.5**	2	0.4	1	0.7

(b) Target: Fe

Ion	H^+	H^+(2MeV)	D^+	He^+	He^+(2MeV)	He^{2+}	He^{2+}(0.6MeV)
$\sigma(10^{-10}\mathrm{nm}^2)$	44.7	0.25	**44.8**	173	1.0	44.3	11.0
R(nm)	624	18,400	**500**	436	3,260	700	1,146
K	0.9355	0.9355	**0.8752**	0.7656	0.7656	0.7656	0.7656
d_a(nm)	200	8,000	**180**	170	1,300	300	480
$r_m(\frac{\Delta E_1}{\Delta M_2})$	0.18	2.5	**0.36**	0.73	10	1.46	3.0
ΔM_2	28	6	**14**	7	1.5	3.5	2.7

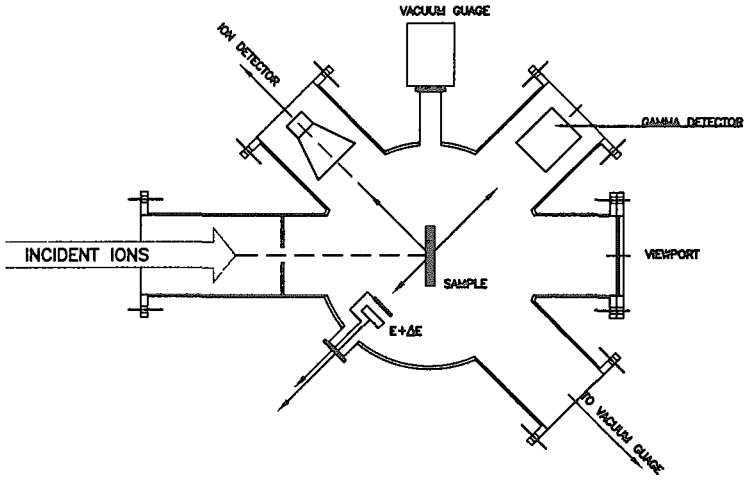

Figure 2: Schematic of the fully-designed 90°-chamber.

3 FEATURES OF THE NEW COMPOSITE FACILITY

Based on the theoretical analysis of the low-energy ion beam RBS, it has been considered that appropriate designing of the new facility is feasible to satisfy the application requirements. The new installations include three parts, an accelerating system and two application chambers. The current 150-kV accelerating capability is to be upgraded to 350 kV. A multiple-purpose chamber containing detecting systems which consist of a time-of-flight charged particle spectrometer and a high resolution gamma-ray system is to replace the old target chamber at the 90°-beam-line terminal, as shown in Figure 2. A TOF-RBS chamber is to be built at the 30°-beam-line terminal, as shown in Figure 3. At the first stage the 90°-chamber is designed only for the pulsed low-energy D-ion beam TOF+RBS analysis, as shown in Figure 4. The new facility to be finally completed is shown in Figure 5.

4 RESOLUTION ANALYSIS

4.1 TOF Method Able to Achieve a Super-High Energy/Mass Resolution

Since the energy, E, of a flying particle (its mass: m) is

$$E = \frac{1}{2}m(\frac{L}{t})^2, \tag{1}$$

where L is the flight path length and t is the flight time from the target to the detector (Figure 4). If Δt is the timing resolution of the spectrometer, then the corresponding energy resolution is

$$\Delta E = \frac{mL^2}{2}[\frac{1}{(t-\Delta t)^2} - \frac{1}{(t+\Delta t)^2}] = \frac{2mL^2 t\Delta t}{[t^2-(\Delta t)^2]^2}. \tag{2}$$

It is noted that $t^2 = \frac{mL^2}{2E}$ and generally $t >> \Delta t$, so the denominator of the above expression can be simplified as t^4. Thus, the final expression for the energy resolution converted from the timing resolution is

$$\Delta E = \frac{4\sqrt{2/m}E^{3/2}}{L}\Delta t. \tag{3}$$

If $m = (1.673+1.675)\times 10^{-27}$ kg (the mass of deuteron), $E = 150$ keV, $L = 0.3$ m, and $\Delta t = 10^2$ ps, the energy resolution calculated from the above formula then becomes around 1 keV. This is just about 1/10 of the energy resolution of conventional RBS. When this resolution is applied to the data in the table above, the resolvable mass difference will be satisfactorily reduced to around 1.

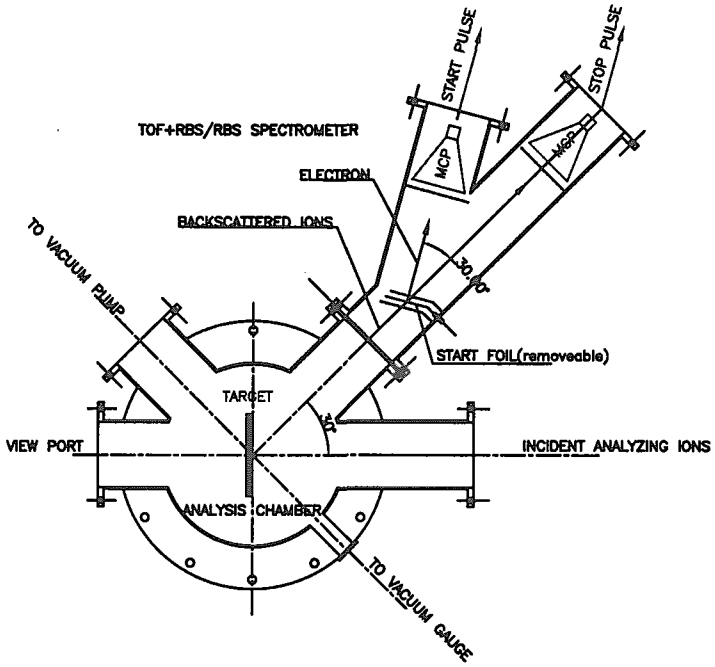

Figure 3: Schematic of the 30°-terminal chamber for the medium-energy ion beam TOF+RBS/RBS analysis.

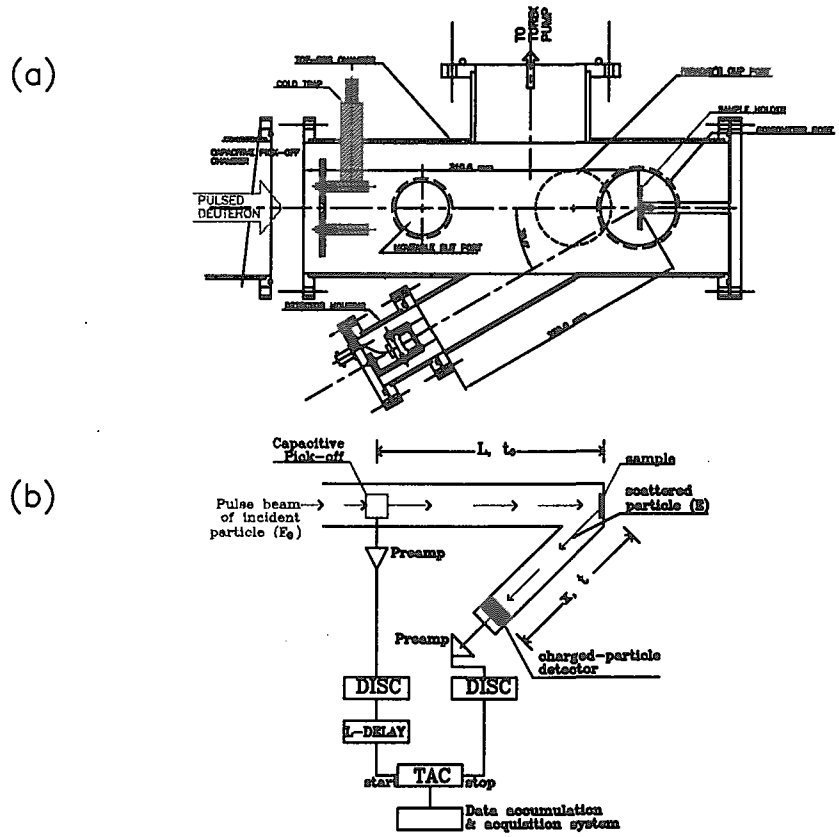

Figure 4: Designing of the pulsed low-energy D-ion beam TOF+RBS analysis. (a) Schematic of the 90°-terminal chamber, (b) the principle of the technique (DISC: discriminator, L-DELAY: logic delay, TAC: time-to-amplitude convertor).

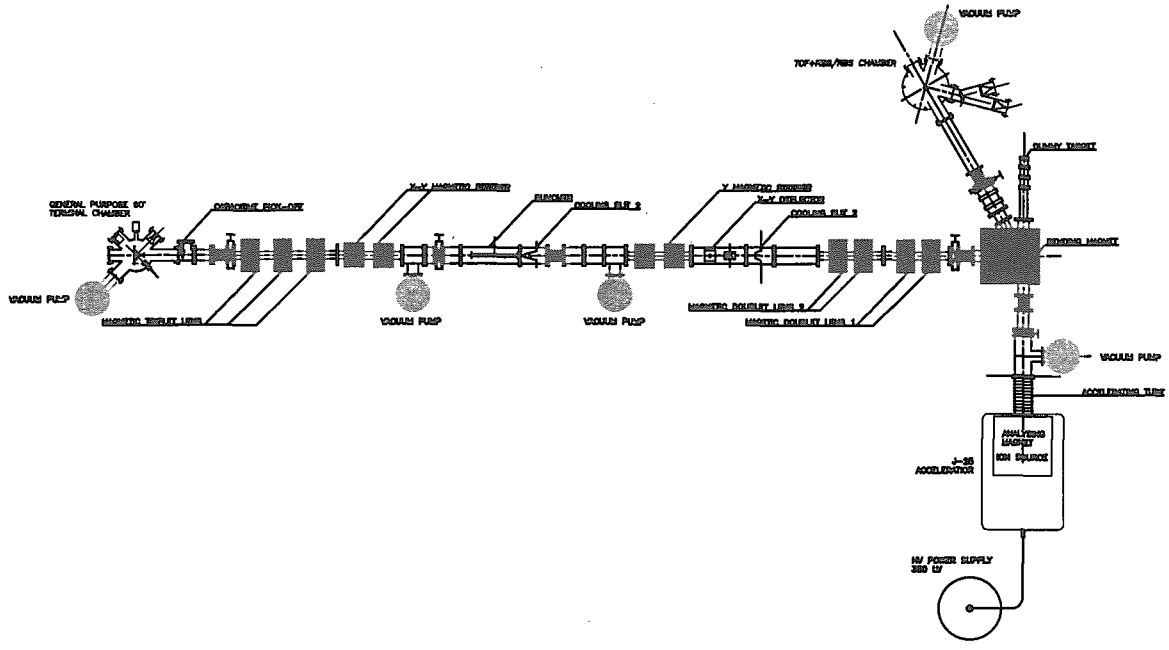

Figure 5: Schematic of the new facility.

4.2 Total System Energy Resolution Analysis (for the low-energy beam line)

The final energy of a backscattered particle detected is

$$\begin{aligned} E_1 &= \frac{m}{2}\frac{L_b^2}{t_b^2} \\ &= \frac{m}{2}\frac{L_b^2}{(t_f - t_c - \Delta t_t)^2}, \end{aligned} \tag{4}$$

where

$$t_c = \sqrt{\frac{m}{2E_0}} L_c, \tag{5}$$

and

$$\begin{aligned} \Delta t_t &= \sqrt{\frac{m}{2E_0}}(l_{in} + \frac{l_{out}}{K^{1/2}}) \\ &= \sqrt{\frac{m}{2E_0}} l_{in}(1 + \frac{1}{K^{1/2}\cos\theta}), \end{aligned} \tag{6}$$

where l_{in} and l_{out} are the path lengths of the analyzing particle travelling-in and travelling-out in the target, respectively, K is the kinematic factor, and θ is the scattering angle.
As discussed before, Δt_t is negligible, then E_1 is simplified as

$$E_1 = \frac{m}{2}\frac{L_b^2}{(t_f - t_c)^2}. \tag{7}$$

The total energy resolution is then approximately

$$\Delta E_1 = \sqrt{(\frac{\partial E_1}{\partial L_b}\Delta L_b)^2 + (\frac{\partial E_1}{\partial t_f}\Delta t_f)^2 + (\frac{\partial E_1}{\partial t_c}\Delta t_c)^2}$$
$$= 2E_1\sqrt{(\frac{\Delta L_b}{L_b})^2 + (\frac{\Delta t_f}{t_f - t_c})^2 + (\frac{\Delta t_c}{t_f - t_c})^2}. \quad (8)$$

As $t_c = \sqrt{\frac{m}{2E_0}}L_c$, which is the actual way t_c is measured, its variance is then

$$(\Delta t_c)^2 = (\frac{\partial t_c}{\partial L_c}\Delta L_c)^2 + (\frac{\partial t_c}{\partial E_0}\Delta E_0)^2$$
$$= (t_c)^2[(\frac{\Delta L_c}{L_c})^2 + \frac{1}{4L_c}(\frac{\Delta E_0}{E_0})^2], \quad (9)$$

where ΔL_c is the uncertainty of the measurement of L_c, and ΔE_0 is the uncertainty of the incident energy, which is dominated by the ripple of the high-voltage generator and the pulse-generation induced energy deviation.
Generally, the uncertainties of the measurements of L_b and L_c are fairly small compared with themselves, i.e. $\Delta L_b/L_b$ and $\Delta L_c/L_c$ are negligible. For ΔE_0, although the ripple of the accelerating voltage is fairly small compared with the high voltage itself, the bunching of the beam to form the pulses causes a 0.2% uncertainty, i.e. $\Delta E_0/E_0 \simeq 2 \times 10^{-3}$. Therefore, besides by Δt_c, the total energy resolution is dominated by Δt_f, which can be expressed by

$$\Delta t_f = \sqrt{(\Delta t_{start})^2 + (\Delta t_{stop})^2 + (\Delta(\Delta t_t))^2}, \quad (10)$$

where Δt_{start} and Δt_{stop} are the uncertainties of measuring the start pulse and the stop pulse, respectively, and $\Delta(\Delta t_t)$ is the timing uncertainty due to the energy straggling of the particle traveling in the target.
The uncertainties of measuring the start pulse and the stop pulse are composed of two factors, which are the uncertainty of the pulse generation and the timing resolution of the detector. So, as the detector only detects the stop pulse,

$$\Delta t_{start} = \sqrt{(\Delta t_{s-pulse})^2} \quad (11)$$

and

$$\Delta t_{stop} = \sqrt{(\Delta t_{s-pulse})^2 + (\Delta t_{s-timing})^2}, \quad (12)$$

where $\Delta t_{s-pulse}$ is the uncertainty of the pulse generation, which is the same for both start pulse and stop pulse, and $\Delta t_{s-timing}$ is the timing resolution of the detector detecting the stop pulse. The uncertainty of the pulse generation is supposed to be proportional to the pulse length, i.e. $\Delta t_{s-pulse} = \alpha l_{pulse}$, where α is the proportional factor and l_{pulse} is the pulse length.
As estimated before, Δt_t is at the order of 10^{-15} s., $\Delta(\Delta t_t)$ is then further smaller, while the timing resolution of a MCP detector is generally at an order of 0.1 ns, or 10^{-10} s., $\Delta(\Delta t_t)$ is neglected. Therefore, basically,

$$\Delta t_f = \sqrt{2(\Delta t_{s-pulse})^2 + (\Delta t_{s-timing})^2}. \quad (13)$$

And now

$$\begin{aligned}\Delta E_1 &\simeq \frac{2E_1}{t_b}\sqrt{(\Delta t_f)^2+(\Delta t_c)^2} \\ &\simeq \frac{2E_1}{t_b}\sqrt{2(\Delta t_{s-pulse})^2+(\Delta t_{s-timing})^2+(\Delta t_c)^2},\end{aligned} \tag{14}$$

where $t_b \simeq t_f - t_c$. Due to $t_b = \sqrt{\frac{m}{2E_1}}L_b$, the above expression then becomes

$$\Delta E_1 = \frac{4E_1^{3/2}}{\sqrt{2m}L_b}\sqrt{2(\Delta t_{s-pulse})^2+(\Delta t_{s-timing})^2+(\Delta t_c)^2}. \tag{15}$$

For example, detection of a backscattered D^+ ($m = (1.673+1.675)\times 10^{-27}$ kg) at an energy of 100 keV ($E_1 = 100\times 10^3 \times 1.6 \times 10^{-19}$ J) at a distance of 0.3 m ($L_b = 0.3$ m) from the target surface using a pulse with the pulse length of 1 ns but a proportional factor α of the uncertainty about 10% and a MCP detector with a timing resolution about 200 ps will have the total energy resolution at about 1.3 keV.

5 CONCLUSION

A low-energy ion accelerator facility (0-350 kV) has been proposed and is being established at Chiang Mai University for high-resolution TOF+RBS analysis, charged particle induced γ-ray and charged particle emission measurement.

ACKNOWLEDGEMENTS

The work is supported by the International Atomic Energy Agency, Vienna, project No. THA/1/009 and the Thailand Research Fund.

References

[1] M.H. Mendenhall and R.A. Weller, Nucl. Instr. and Meth. B47(1990)193.

[2] W-K. Chu, J.W. Mayer and M-A. Nicolet, Backscattering Spectrometry, Academic Press, New York, 1978.

[3] T. Vilaithong, S. Singkarat, W. Pairsuwan, JF. Kral, D. Boonyawan, D. Suwannakachorn, S. Konklong, P. Kanjanarat, and G.G. Hoyes, Int. Cong. on Nuclear Data for Science and Technology, May 13-17, 1991, Julich, Germany, pp.483-486.

[4] J.F. Ziegler, Helium Stopping Powers and Ranges in All Element Matter, Pergamon Press, New York, 1977.

[5] H.H. Andersen and J.F. Ziegler, Hydrogen Stopping Powers and Ranges in All Elements, Pergamon Press, New York, 1980.

[6] J.F. Ziegler, Handbook of Stopping Cross-Sections for Energetic Ions in All Elements, Pergamon Press, New York, 1980.

[7] Yu Liangdeng, Diffusion of Ions Implanted in Solids, Ph.D. Series 1992-02, University of Copenhagen, ISSN 0906-0286 (1992).